# The relative importance of domain size, domain purity and domain interfaces to the performance of bulk-heterojunction Organic Photovoltaics.

*Benjamin P. Lyons*[*], *Nigel Clarke*[†], *Chris Groves*[*]

[*] School of Engineering and Computing Sciences, Durham University, South Road, Durham, DH1 3LE, United Kingdom.

[†] Department of Physics and Astronomy, Sheffield University, Hounslow Road, Sheffield, S3 7RH, United Kingdom.

*e-mail*: n.clarke@sheffield.ac.uk (N.C.), chris.groves@durham.ac.uk (C.G.)

TABLE OF CONTENTS ENTRY

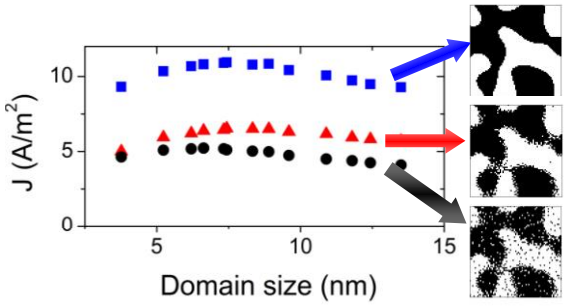


A combination of Cahn-Hilliard and Monte Carlo modeling is used to investigate the relative importance of size, purity and interfaces of domains to the performance of bulk heterojunction Organic Photovoltaics.

## BROADER CONTEXT

Photovoltaic devices fabricated from solution-processable conjugated polymers and small molecules (OPVs) offer the possibility of dramatically reducing the cost of renewable energy. The efficiency of such devices has increased very rapidly in recent years and is currently very close to 10%. A wide range of studies suggest that one of key factors in obtaining high performance is the morphology of the donor-acceptor network within the active layer. However, it is not entirely clear what aspects of the morphology are most important to their performance due to the difficulty of demonstrating causal links between properties and performance. As a result, the relative importance of size and purity of domains, and the interfaces between, is not generally known. In this paper we use morphological and charge transport modeling techniques to show unambiguously the effect of these features on the performance of OPVs. Surprisingly we find that the commonly reported 'optimum' domain size of ~10nm is only of significant benefit in structures with pure domains, and further that sharpening the interface between domains is of greater benefit to performance. We also show how changing the interaction parameter of the blend components is a versatile technique to achieve sharper interfaces and higher OPV performance. More generally, we have demonstrated a combination of modeling techniques that are able to give an indication of answers to questions relevant to OPVs that would be difficult to achieve experimentally.

## ABSTRACT

The domain size, domain purity and interfacial width between domains for a bulk heterojunction are controllably altered through use of Cahn-Hilliard modeling and their relative effect on OPV performance is predicted using Monte Carlo modeling. It is found that locally-sharp, well-connected domains of only 4nm extent out perform morphologies with broadened interfaces and/or impure domains even when domain sizes were at the 'optimum' size of ~10nm. More generally, these data provide information on the most effective method to optimize the as-cast bulk heterojunction morphology depending upon initial domain purity and the nature of interfaces between domains. Further, it indicates why morphology optimization is more effective for some blends than others. It is shown that the quench depth of the blend can be used as a general technique to control the interfacial structure of the morphology and realize substantial increases in short circuit photocurrent.

KEYWORDS: Bulk heterojunction solar cells, Monte Carlo simulation, Cahn-Hilliard techniques, organic photovoltaics, charge transport, bulk heterojunction

## 1. INTRODUCTION

Conjugated polymers and fullerene derivatives have a number of properties that make them good candidates for use as active materials in a photovoltaic device. In particular, solution-processability opens up the possibility of low-cost and high-throughput printing[1], whilst chemical tunability offers the opportunity to match their absorption spectrum to sunlight[2]. Unfortunately these advantages are tempered by a large exciton binding energy[3], meaning that absorbed photons do not readily yield free charges that can do useful work in an external circuit. Viable photovoltaics made from these organic materials (OPVs) are however made possible without sacrificing scalable manufacturability by an internal structure known as a bulk-heterojunction[4, 5]. A bulk heterojunction can be formed relatively simply by casting or printing a solution of two materials having different ionization potentials. When the solvent evaporates, a finely mixed donor-acceptor network which weaves its way through a ~100nm thick film can result. The finely mixed donor-acceptor network allows efficient exciton dissociation, whilst the thick film allows efficient light absorption. However, whilst the bulk heterojunction has made charge generation efficient enough for OPVs to be feasible, they also hamper charge transport[6, 7], meaning there is an inherent tension between the competing morphological needs of charge generation and charge extraction. Indeed, shortly after the first bulk heterojunction OPVs were reported it was shown that changes in the donor-acceptor morphology could significantly affect the performance[8, 9], and more than a decade of research has followed to reconcile these competing needs.

Fortunately, much progress has been made towards this goal as a wide range of factors have been shown to affect OPV morphology and performance, including changing solvent[8], rate of solvent evaporation[9], blend ratio[10], regioreularity[11], polymer design[12], thermal annealing[13, 14], solvent vapor annealing[15], and the use of additives[16], to name a few. This large body of experimental work, which is

additionally reviewed in these papers[17-24], has suggested a picture of what an 'ideal' OPV morphology might be. Although there are regional variations, usually this 'ideal' includes phase separation on the lengthscale of ~10nm to match the typical exciton diffusion length[25] with abrupt transitions between pure donor and acceptor phases. Furthermore, 'ideal' donor and acceptor networks have perfect connectivity to anode and cathode respectively, possibly via straight paths to the electrodes. Needless to say, achieving this 'ideal' in its entirety is very challenging using a solution-processed approach and has yet to be reported.

If it is only possible to partly achieve these morphology ideals, this raises the question of which are most beneficial to OPV performance. For example, is it better to strive for better connectivity to the electrode, or to have a domain size of ~10nm? How important is interfacial roughness between domains compared to domain size? Does a finely mixed morphology prohibit good photovoltaic performance? While experiments can provide partial answers to these questions (for example[26]), it is generally not possible to compare the whole range due to the difficulty of independently controlling one morphological feature whilst keeping others constant. The resultant lack of information makes optimization of OPVs and the analysis of the optimization process challenging. In particular, it is often not clear what route one should take to try and optimize the morphology, since many routes are possible and not all result in improved performance[27]. Furthermore, understanding why optimization is more effective for some OPV blend systems[8] than others[28] is often unclear and requires laborious experimentation to discover why.

In this paper we use a joint modeling approach to show unambiguously how various aspects of morphology affect OPV performance. We find that annealing blends with impure domains is relatively ineffective because improvement in charge separation efficiency is balanced by reducing connectivity to the electrode. Furthermore, and perhaps most surprisingly, sharp interfaces between domains are predicted to have a substantial benefit to charge collection efficiency, with blends with sharp interfaces and only 4nm domains out-performing a blend with 'optimal' ~10nm domains with diffuse interfaces. Being able to examine how these individual aspects of morphology affect performance reveals the most effective method to improve OPV performance depending upon the morphology type. We also show that

changing the interaction parameter, for example by using an additive, is an effective technique to improve performance for all morphology types considered.

## 2. CAHN-HILLIARD AND MONTE CARLO SIMULATIONS

Morphologies for use in the Monte Carlo charge transport simulation were generated using a modified Cahn-Hilliard approach described in detail elsewhere[29-31] and in the supplementary information. Briefly, the morphology is represented by a Cartesian lattice extending 128nm in each direction with a lattice spacing of 1nm. Each site has an associated fraction of donor material, $\phi$ which is initially assumed to be $0.5 + \delta$ at all locations, where $\delta$ is a randomly chosen perturbation in the range $-0.01 < \delta < 0.01$ to 'seed' the morphology. This homogeneous blend is quenched into the two-phase region whereupon phase separation proceeds over a dimensionless 'annealing time', $\tau_{anneal}$. The parameters used for the Cahn-Hilliard simulations are shown in the supplementary information. It was assumed that the molecular weight of donor and acceptor were equal, similar to all-polymer OPVs. Of course, phase separation in organic photovoltaic systems is usually a consequence of solvent evaporation and thermal annealing. The modeling of evaporation driven processes is still at an early phase, and much of the relevant physics is only beginning to be discovered[32]. Hence we here use a temperature quench as a convenient method for producing qualitatively realistic phase-separated structures. This said, we also note that the Cahn-Hilliard technique describes more completely the thermodynamics and kinetics of morphology evolution than Ising methods which have been used previously to simulate bulk heterojunction morphology evolution[33-35].

The result of Cahn-Hilliard modeling is a Cartesian grid of sites with continuously varying $\phi$ that represents the local composition. For Monte Carlo modeling it is necessary that each site has a definite character, i.e. they must either be a donor or acceptor, and so further processing is required. Here we use three different processing algorithms to give us control over aspects of the morphology, and in doing so we are able to assign their relative importance to OPV performance. The first algorithm, which we term the compositional interpretation (CI), considers $\phi$ as the probability that a particular site is a donor. A

random number between 0 and 1, $x$ is generated for each site, and any site with $x \leq \phi$ is assigned as donor. A CI morphology, shown in figure 1a, is characterized by impure domains and rough interfaces between domains. The second algorithm, which we term the diffuse interface interpretation (DII), takes the CI morphology and swaps from donor to acceptor any donor site which has fewer than two nearest neighbor donor sites, and vice versa for acceptor sites. DII morphologies, as shown in figure 1b, are characterized by largely pure domains, as any isolated donor or acceptor sites are removed, and diffuse interfaces between domains. The final algorithm, which we term the sharp interface interpretation (SII), assigns any site with $\phi < 0.5$ as donor, and the rest as acceptor. This in turn gives a morphology with completely pure domains and sharp interfaces, as shown in figure 1c.

This approach is qualitative rather than quantitative, as our aim here is to examine relative importance of general morphological features present in OPV devices rather than specific examples. Our approach of using Cahn-Hilliard morphologies allows us to describe more realistically the thermodynamics and kinetics of polymer blend phase separation more realistically that the Ising methods used previously[33-35], which produce morphologies similar to the 'idealized' SII morphology. Furthermore, the algorithms used allow us to examine the consequences of impure domains (CI) and broadened interfaces between domains (DII) shown to occur in real devices. This said, it is important to note that here we do not take into account of the nature of polymer chains[36, 37], and that the single quench used here results in morphologies with a single characteristic domain size, rather than a heterogeneous distribution commonly reported[27, 38, 39].

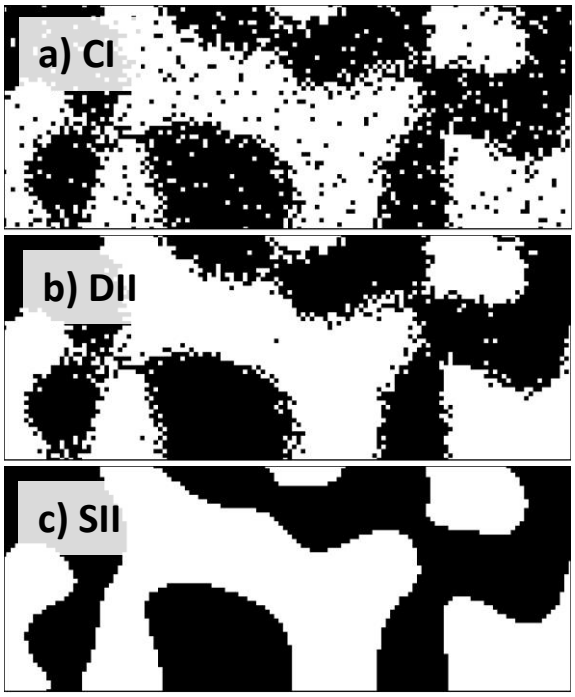


**Figure 1:** 2D images of an x-y slice through a morphology when processed by (a) the compositional interpretation, CI, (b) the diffuse interface interpretation, DII and (c) the sharp interface interpretation, SII. Black represents donor and white represents acceptor. Note that the figure is zoomed in onto a 127nm×50nm rectangle to show detail of the small features.

We quantify the properties of these morphologies by calculating their pair distribution function[40], $P(R)$, which is defined as the probability that two sites picked at random and separated by a distance $R$ will be of the same type (i.e. whether they are both donor or both acceptor). At small values of $R$, the pair distribution function is indicative of the size and purity of domains, while at large values of $R$ it probes bulk blend composition. Figure 2 shows $P(R)$ for the CI, DII and SII morphologies when $\tau_{anneal} = 40$ and 400. The average domain size, $d$ is given by the value of $R$ at which $P(R)$ first drops to the bulk composition of $\phi = 0.5$. It can be seen that the domain size does not depend not on the algorithm used, but does increase with the degree of annealing, as expected. Morphologies with $10 \leq \tau_{anneal} \leq 400$ are examined which in turn correspond to domain sizes of $4\text{nm} \leq d \leq 14\text{nm}$, therefore covering a wide part of the range over which optimal performance is expected in OPVs[41, 42]. Figure 2 also indicates the internal

structure of the domains, with domain purity being greatest for the SII algorithm, followed by DII and then CI algorithms. Figure 2 also shows that the domains are surrounded, to some extent, by a 'halo region' which is richer in the opposite material to the domain when compared to the bulk (i.e. $P(R) < 0.5$). Such halo regions are a result of growing domains expelling the opposite material type, and have been observed in polyfluorene:fullerene OPV systems[43]. Importantly, it can be seen that the various algorithms have not affected the bulk composition, as $P(R)$ converges to 0.5 at large values of $R$ for all cases.

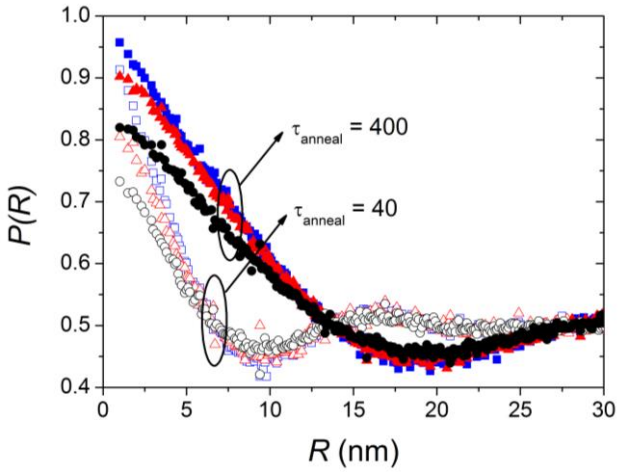


**Figure 2:** Pair distribution function, $P(R)$ for Cahn-Hilliard morphologies with $\tau_{anneal} = 40$ (open symbols) and 400 (closed symbols). CI, DII and SII interpretations of the morphology are denoted by black circles, red triangles and blue squares respectively.

The Monte Carlo technique used here to predict OPV performance is described in detail elsewhere[31, 35, 44, 45] and in the supplementary information, and so only a brief summary will be given here. Each site in the morphology is additionally assigned a Gaussian-distributed energy to simulate the effects of energetic disorder. Singlet excitons are created at random locations and move via Förster transfer with a rate determined by both site separation and the energy difference. If excitons travel to a donor-acceptor boundary, they immediately dissociate into an electron-hole pair. Charges may hop to a nearest neighbor site of the appropriate material (electrons to acceptors and holes to donors) at a rate given by a Marcus expression, or recombine at a constant rate if adjacent. The hopping rate calculation includes the internal electric field, all Coulombic interactions between charges and image charges, and the

polaronic re-organization energy. Like the Cahn-Hilliard simulations, parameters were chosen to be appropriate for all-polymer OPVs[31], and are shown in the supplementary information. We note that the parameters used for the charge transport simulation are similar to those which gave quantitative agreement with polymer-polymer bilayer OPVs[26]. Since we are examining the relationship between morphology on photocurrent generation, we do not include dark injection at the contacts[46].

## 3. EXAMINING THE EFFECT OF DIFFERENT MORPHOLOGY INTERPRETATIONS ON OPV PERFORMANCE

Figure 3 shows simulated current densities at a field of $1\times10^7$ V/m, corresponding approximately to short circuit in an OPV, when $10 \leq \tau_{anneal} \leq 400$ for each of the CI, DII and SII interpretations of the morphology. The exciton dissociation efficiency, $\eta_{EX}$, and the carrier collection efficiency, here defined as the efficiency with which a photogenerated charge reaches the collecting electrodes, $\eta_{CC}$, are also shown (plots of the geminate and bimolecular recombination efficiency are shown in the supplementary information). Recall that the underlying Cahn-Hilliard morphology for a given domain size of SII, DII and CI morphology is the same, and so difference in performance is due to changes in domain purity, interfacial roughness and connectivity only. To begin with, all of the different morphologies show optimum photocurrent (top panel) at a domain size of around 7nm, where the competing needs of efficient exciton dissociation (middle panel) and charge collection (bottom panel) are balanced[33, 41]. This optimum domain size agrees well with recent Resonant soft X-Ray Scattering (R-SoXRS) data for all-polymer OPVs[39].

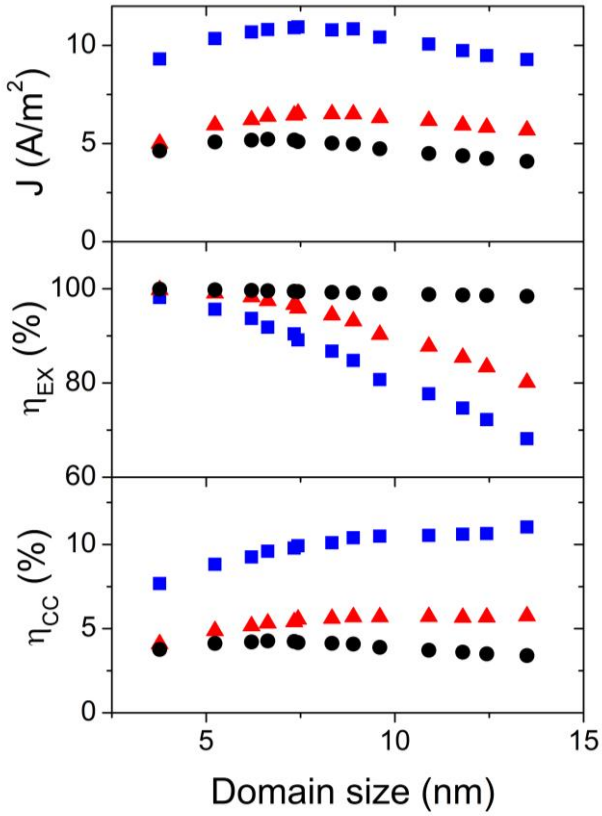


**Figure 3:** Simulated current density (top), exciton dissociation efficiency (middle) and carrier collection efficiency (bottom) as a function of domain size for morphologies as interpreted by the CI (black circles), DII (red triangles) and SII (blue squares) algorithms.

3.1 Contrasting the effect of annealing in morphologies with impure and pure domains

It is apparent that the PV performance of the SII and DI morphologies, with comparatively pure domains, are affected more by changing domain size than the CI morphology, which has impure domains. Indeed, the carrier collection efficiency ($\eta_{CC}$) for the CI morphology changes by a factor of only 15% over the range considered, and actually drops at large *d*. It is relatively straightforward to investigate why this is the case by logging additional information in the Monte Carlo model, and in particular, the connectivity offered by the morphology. To do this we first determine for each site in the simulation volume whether a nearest-neighbor hopping route is available to the appropriate electrode. We thereafter log the connectivity that each charge pair has in the simulation when it is created, and gather statistics of the charge pair behavior depending upon what type of connectivity it has. We consider three populations

of charge pairs; *all* charge pairs, charge pairs where *both* the electron and hole have a possible route to the collecting electrodes, and charge pairs where *only one* charge has a possible route to the collecting electrode. For brevity, we hereafter denote these populations respectively as; all pairs, pairs with good connectivity, and pairs with poor connectivity. Note that there is also a population of charge pairs where neither charge has a route to the electrode, but these are small in number (<0.5% of the population) and so are ignored here.

Figure 4 shows the carrier collection efficiency for all charges, charges with good connectivity and poor connectivity for an optimal ($\tau_{anneal}$ = 40) and an over-annealed blend ($\tau_{anneal}$ = 400) for each algorithm. It can be seen that annealing increases the carrier collection efficiency of each population of charges (good and poor connectivity), as might be expected due to the increased entropic driving force for charge separation[26, 42, 47]. The collection efficiency for charges with poor connectivity is substantially lower than for those with good connectivity, as might be expected, but is non-zero since one carrier can leave via the contacts (although obviously this leaves behind an uncompensated charge which can lead to bimolecular recombination elsewhere[48]). These trends are all evident for the CI, DII and SII morphologies. Now focusing on the CI morphology alone, even though collection efficiency *for a given population of charges* may increase with annealing, there is also a substantial reduction in the proportion of charges created with good connectivity (from ~55% to ~30%). These counteracting mechanisms explain why the OPV photocurrent changes comparatively little upon annealing in the CI morphology.

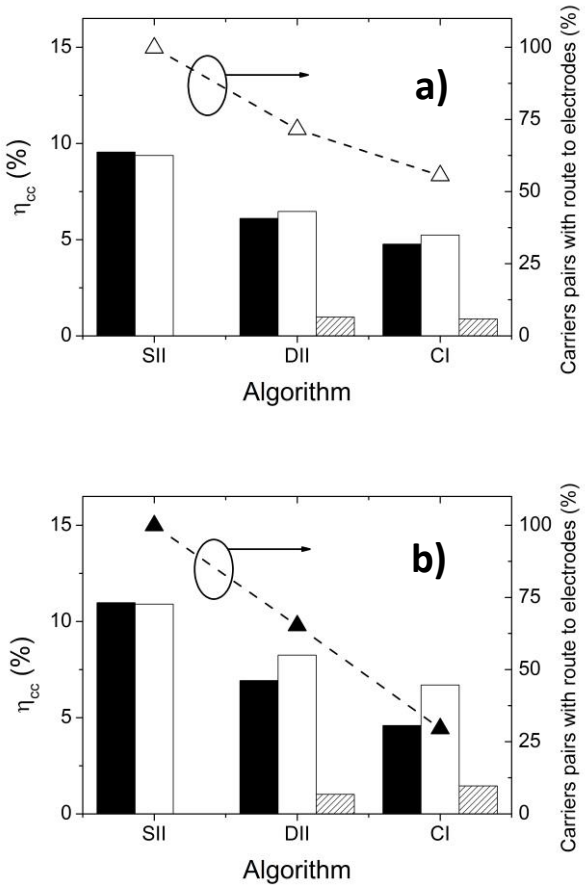


**Figure 4:** Simulated carrier collection efficiency, $\eta_{CC}$ for morphologies with (a) $\tau_{anneal}$ = 40 and (b) $\tau_{anneal}$ = 400, interpreted using each of the SII, DII and CI algorithms. The filled, open and hashed bars respectively denote $\eta_{CC}$ for all charge pairs, charge pairs in which both carriers are connected to the appropriate electrodes, and charge pairs when only one carrier is connected to the appropriate electrode. Symbols show the percentage of charge pairs created with good connectivity. Note that >99.9% of charges in the SII morphologies were created with good connectivity and so an accurate carrier collection efficiency for charges with poor connectivity could not be measured.

This is contrasted with the SII and DII morphologies which have pure domains. Figure 3 shows that the effect of annealing on the ensemble of all charges is more significant in this case, as $\eta_{CC}$ increases by a factor of ~45% for both the SII and DII morphologies when *d* increases from 4nm to 14nm. The anticipated benefit of annealing is realized here because annealing is not associated with substantial drops

in connectivity to the electrode (figure 4). This indicates that maintaining good connectivity during annealing is a pre-requisite for realizing the expected benefits to collection efficiency[26, 42, 47].

3.2 Comparing sharp and diffuse domain interfaces

We can examine the effect of the interface between domains upon PV performance by comparing the SII and DII morphologies, which have sharp and diffuse interfaces respectively. The difference in performance shown in figure 3 is striking, with the SII morphology having carrier collection efficiencies approaching twice that of the DII morphology. The overall result of which is that an SII morphology with a domain size of only ~4nm gives almost 50% more photocurrent than a more vigorously annealed DII blend with a domain size of ~10nm. These data therefore strongly suggest that improving the order in the region of the interface in a finely mixed morphology is of greater benefit to PV performance than optimizing the domain size.

We can again investigate the reasons for this further by examining the behavior of populations of charges with good and poor connectivity as shown in figure 4. For a given degree of annealing charges with good connectivity in the SII morphologies give greater collection efficiency by a factor of 20-30% than the DII morphologies. Hence the diffuse interfacial structure does indeed reduce the degree of entropy driving charge separation[26] (geminate recombination efficiency is shown in figure S2 of the supplementary information). However, it can also be seen that the diffuse interface also leads to a smaller proportion (an absolute reduction of ~25%) of charges created with good connectivity. The reduction in performance between the SII and DII morphologies is therefore due in roughly equal measure to a reduction in charge separation efficiency for charges with good connectivity and a reduction in the proportion of charges with good connectivity.

3.3 Relation to experiment

The CI data presented here most closely simulates OPV performance of morphologies with impure domains that may result when donor and acceptor are highly miscible. However, we must be cautious in interpreting the current data to ensure we do not over-generalize, particularly because the

physics used to describe phase separation is only qualitatively analogous to that which occurs in real devices, as discussed in section 2. Along these lines, it is important to note that miscibility is here accompanied by poor electrode connectivity which may not occur for all blend systems. In particular, Phenyl-$C_{61}$-butyric acid methyl ester (PCBM) is highly miscible in poly(3-hexlythiophene) (P3HT)[49] but optimized blends of P3HT:PCBM show good photovoltaic performance[13], indicative that good connectivity should be present[50]. Interestingly, P3HT:PCBM blends require a slight excess of PCBM with respect to the eutectic point to obtain optimum performance[10], perhaps indicating a small amount of PCBM is needed to 'join up' the molecular PCBM routes that would otherwise be unconnected to the electrodes. These caveats aside, there are a number of (typically all-polymer[10]) blend systems in which miscibility and a small effect of annealing on OPV performance has been reported. For example, all-polymer blends using a Napthalenediimide-based acceptor have been shown to have impure domains for a wide range of annealing conditions and solvents[28, 39], and devices made from similar films show disappointing performance despite the high mobility of the Napthalenediimide-based acceptor. Blend films of poly(9,9-dioctylfluorene-2,7-diyl-1,4-phenylene-bis(N-(p-sec-butylphenyl)imino-1,4-phenylene)) (PFB) and poly(9,9-dioctylfluorene-2,7diyl-benzo-2,1,3-thiadiazole-4,7-diyl) (F8BT) when cast from chloroform also show mixing on molecular lengthscales both before and after annealing[40]. Again, devices made from these materials show only modest changes in performance with annealing[41]. More substantial improvements in PV performance in such miscible blends have been realized using novel techniques that result in purer domains, such as imprinting[51] and crosslinking[52]. The current data also shows this, since purifying the domains (i.e. moving from a CI to DII morphology) increases the PV performance more than changing the domain size of impure domains (i.e. annealing the CI morphology).

By comparison, sharpening the interfaces between domains (i.e. moving from a DII to SII morphology) is predicted to have a greater effect on OPV performance than changing domain size (i.e. annealing either a CI or DII morphology). In the case of the current simulations, this is due in almost equal measure to improved connectivity and increased separation efficiency for carriers that are connected to an electrode. Our data suggests that the effect is sufficiently strong as to make a finely-

mixed 4nm blend with sharp interfaces outperform an 'optimally' annealed blend with diffuse interfaces. We might expect semi-crystalline materials to lead to locally sharp interfaces[17], and indeed there is a wide variety of experimental data linking the onset of crystallization of one blend component with improved charge generation efficiency[53, 54]. However, since domain size also increases on the onset of crystallization[27] as well as other factors that may assist charge generation[55], sharpening the interface is likely to be only part of a larger picture.

Perhaps more importantly, the current data suggest the most effective routes to optimizing the morphology in bulk heterojunction OPVs. Since it is often the case that optimized devices when cast have a morphology which is 'too fine' and require additional solvent[15] or thermal[13, 14] annealing, we assume that the starting point for optimization is a finely mixed blend. If the morphology does not provide good connectivity, for example as in some all-polymer blends[28, 41], then annealing will only have a small effect because improvement in charge separation efficiency will be offset by increased charge trapping. Greater gains in performance in this circumstance will be yielded by attempting to purify the domains or otherwise improving connectivity. If instead the morphology provides good connectivity, as appears to be the case for hypoeutectic P3HT:PCBM blends[10], then the greatest benefit will be obtained by first sharpening the domain interfaces. While increasing the size of the domains to the 'optimal' ~10nm size does improve OPV performance, its effect in comparison to sharpening the domain interface is relatively weak.

## 4. INFLUENCING THE MORPHOLOGY

Of course performing Cahn-Hilliard simulations and then applying different algorithms to obtain an optimal morphology is far more convenient and likely to succeed than is generally the case experimentally. While we have shown that maintaining connectivity to the electrode is important during processing of the OPV film, the techniques to achieve this will depend on whether the donor and acceptor are polymers, small molecules, or a combination[10]. The finding that sharpening the interface between domains improves PV performance is, however, more amenable to making suggestions as to how to improve PV devices in general. The interfacial width between domains in a polymer melt varies as[56] $\sim \chi^{-}$

$^{0.5}$, where $\chi$ is the interaction parameter between the two components of the blend. Unfortunately, at this point it is not generally known how $\chi$ varies with processing parameters, such as temperature, for OPV blend systems. This underlines the need for further characterization of blend forming properties of OPV systems.

However, since Cahn-Hilliard modeling describes morphologies in terms of $\chi$, it is possible for us to make variations in $\chi$ in a way that may be experimentally accessible, and test the effect on OPV performance. Figure 5 shows simulated current densities at a field of $1\times10^7$ V/m when $10 \leq \tau_{anneal} \leq 400$ when the quench depth is $\chi$ = 0.05, 0.065 and 0.08, which hereafter we refer to as the shallow, moderate and deep quench, respectively. In the spirit of trying to show what is experimentally achievable with this approach, we use the CI algorithm to interpret the morphologies since this represents the smallest amount of post-processing. As previously, the domain size for each blend is calculated using the pair distribution function (as in figure 2). It can be seen that the collection efficiency of charges increases by 30% by varying $\chi$ over this range, a substantial benefit achieved even though CI morphologies have poor connectivity.

A method to control $\chi$ that has seen increasing use over recent years is the use of additives which are a good solvent for one component and a poor solvent for the other[12, 16, 57, 58]. It is interesting to note that some of the largest improvements in PV performance reported through use of additives are for blends of semi-crystalline and amorphous polymers[58]. In this case, the additive assists in the formation of polymer crystals, thereby also purifying domains. We speculate that semi-crystalline-amorphous polymer blends generally have more to benefit from additives since they perform two functions, i.e. promoting domain purity and sharpening domain interfaces (corresponding to transition from a CI type morphology to an SII type morphology).

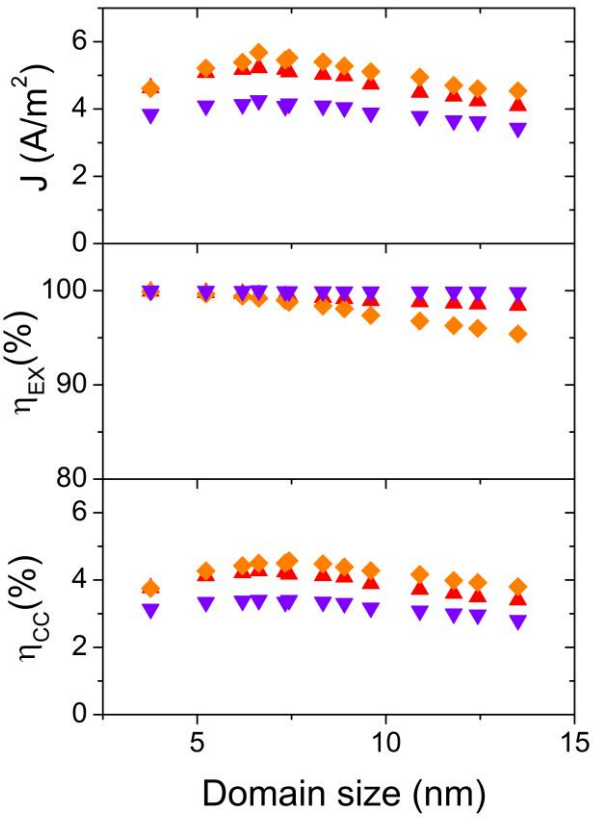


**Figure 5:** Simulated current density (top), exciton dissociation efficiency (middle) and carrier collection efficiency (bottom) as a function of domain size for morphologies with a shallow (purple down triangles), moderate (red triangles) and deep (orange diamonds) quench.

## 5. CONCLUSIONS

We have used a combined modeling approach which allows us to unambiguously examine the relative effect of domain size, domain purity and interfacial character in a bulk heterojunction on OPV performance. These data have shown that varying the domain size for morphologies with impure domains has little effect on performance because the benefit of improved charge separation of carriers with good connectivity to the electrode is offset by an increase in charge trapping. In the case of a miscible blend these data therefore suggest that the greatest benefit to PV performance will be obtained by first purifying the domains, thereby improving connectivity to the electrode, rather than coarsening the

blend. Morphologies with pure domains, by contrast, are shown to have a more pronounced peak in PV performance when the domain size balances the competing needs of charge separation and exciton dissociation. However, it was also shown that first sharpening the interface between domains has a much greater benefit to PV performance than coarsening the domain size in a blend with initially diffuse interfaces. This shows that blend morphologies even with feature sizes below the usually quoted 'optimum' of ~10nm can show good performance provided that the interfaces between domains are sharp. The sharpness of the interface can be controlled via the interaction parameter, which in turn can be controlled through use of additives to the blend solution. By controlling the interaction parameter in our Cahn-Hilliard simulation over the range $0.05 \leq \chi \leq 0.08$ we have shown that improvements in photocurrent by ~30%, even in morphologies with impure domains and poor electrode connectivity, highlighting the usefulness of the additive approach.

ACKNOWLEDGEMENTS

The Monte Carlo simulations were carried out on Durham University's high performance computing cluster, Hamilton.

## REFERENCES

1. A. C. Arias, J. D. MacKenzie, I. McCulloch, J. Rivnay and A. Salleo, *Chem. Rev.*, 2010, **110**, 3-24.
2. J. W. Chen and Y. Cao, *Acc. Chem. Res.*, 2009, **42**, 1709.
3. J. L. Bredas, J. Cornil and A. J. Heeger, *Adv. Mater.*, 1996, **8**, 447.
4. J. J. M. Halls, C. A. Walsh, N. C. Greenham, E. A. Marseglia, R. H. Friend, S. C. Moratti and A. B. Holmes, *Nature*, 1995, **376**, 498.
5. G. Yu, J. Gao, J. C. Hummelen, F. Wudl and A. J. Heeger, *Science*, 1995, **270**, 1789.
6. C. Groves, L. J. A. Koster and N. C. Greenham, *J. Appl. Phys.*, 2009, **105**, 094510.
7. L. J. A. Koster, *Phys. Rev. B*, 2010, **81**, 205318.
8. S. E. Shaheen, C. J. Brabec, N. S. Sariciftci, F. Padinger, T. Fromherz and J. C. Hummelen, *Appl. Phys. Lett.*, 2001, **78**, 841.
9. J. J. M. Halls, A. C. Arias, J. D. MacKenzie, W. Wu, M. Inbasekaran, E. P. Woo and R. H. Friend, *Adv. Mater.*, 2000, **12**, 498.
10. C. Müller, T. A. M. Ferenczi, M. Campoy-Quiles, J. M. Frost, D. D. C. Bradley, P. Smith, N. Stingelin-Stutzmann and J. Nelson, *Adv. Mater.*, 2008, **20**, 3510.

11. Y. Kim, S. Cook, S. M. Tuladhar, S. A. Choulis, J. Nelson, J. R. Durrant, D. D. C. Bradley, M. Giles, I. McCulloch, C. S. Ha and M. Ree, *Nat. Mater.*, 2006, **5**, 197.
12. M. Morana, H. Azimi, G. Dennler, H. J. Egelhaaf, M. Scharber, K. Forberich, J. Hauch, R. Gaudiana, D. Waller, Z. H. Zhu, K. Hingerl, S. S. van Bavel, J. Loos and C. J. Brabec, *Adv. Funct. Mater.*, 2010, **20**, 1180.
13. X. N. Yang, J. Loos, S. C. Veenstra, W. J. H. Verhees, M. M. Wienk, J. M. Kroon, M. A. J. Michels and R. A. J. Janssen, *Nano Lett.*, 2005, **5**, 579.
14. F. Padinger, R. S. Rittberger and N. S. Sariciftci, *Adv. Funct. Mater.*, 2003, **13**, 85.
15. G. Li, Y. Yao, H. Yang, V. Shrotriya, G. Yang and Y. Yang, *Adv. Funct. Mater.*, 2007, **17**, 1636.
16. T. Agostinelli, T. A. M. Ferenczi, E. Pires, S. Foster, A. Maurano, C. Muller, A. Ballantyne, M. Hampton, S. Lilliu, M. Campoy-Quiles, H. Azimi, M. Morana, D. D. C. Bradley, J. Durrant, J. E. Macdonald, N. Stingelin and J. Nelson, *J. Polym. Sci. Pt. B-Polym. Phys.*, 2011, **49**, 717.
17. C. R. McNeill, *Energy Environ. Sci.*, 2012, **5**, 5653.
18. H. Hoppe, M. Niggemann, C. Winder, J. Kraut, R. Hiesgen, A. Hinsch, D. Meissner and N. S. Sariciftci, *Adv. Funct. Mater.*, 2004, **14**, 1005.
19. B. C. Thompson and J. M. J. Fréchet, *Angewandte Chemie International Edition*, 2008, **47**, 58.
20. C. R. McNeill and N. C. Greenham, *Adv. Mater.*, 2009, **21**, 3840.
21. C. J. Brabec, M. Heeney, I. McCulloch and J. Nelson, *Chem. Soc. Rev.*, 2011, **40**, 1185.
22. L. M. Chen, Z. R. Hong, G. Li and Y. Yang, *Adv. Mater.*, 2009, **21**, 1434.
23. J. Peet, A. J. Heeger and G. C. Bazan, *Acc. Chem. Res.*, 2009, **42**, 1700.
24. A. J. Moulé and K. Meerholz, *Adv. Funct. Mater.*, 2009, **19**, 3028.
25. S. R. Scully and M. D. McGehee, *J. Appl. Phys.*, 2006, **100**, 034907.
26. H. Yan, S. Swaraj, C. Wang, I. Hwang, N. C. Greenham, C. Groves, H. Ade and C. R. McNeill, *Adv. Funct. Mater.*, 2010, **20**, 4329.
27. R. C. Nieuwendaal, H. W. Ro, D. S. Germack, R. J. Kline, M. F. Toney, C. K. Chan, A. Agrawal, D. Gundlach, D. L. VanderHart and D. M. Delongchamp, *Adv. Funct. Mater.*, DOI: 10.1002/adfm.201102138.
28. J. R. Moore, S. Albert-Seifried, A. Rao, S. Massip, B. Watts, D. J. Morgan, R. H. Friend, C. R. McNeill and H. Sirringhaus, *Adv. Energy Mater.*, 2011, **1**, 230.
29. I. C. Henderson and N. Clarke, *Macromol. Theory Simul.*, 2005, **14**, 435.
30. J. Fukuda, M. Yoneya and H. Yokoyama, *Phys. Rev. E*, 2006, **73**, 066706.
31. B. P. Lyons, N. Clarke and C. Groves, *J. Phys. Chem. C*, 2011, **115**, 22572.
32. K. R. Thomas, A. Chenneviere, G. Reiter and U. Steiner, *Phys. Rev. E*, 2011, **83**, 021804.
33. P. K. Watkins, A. B. Walker and G. L. B. Verschoor, *Nano Lett.*, 2005, **5**, 1814.
34. R. A. Marsh, C. Groves and N. C. Greenham, *J. Appl. Phys.*, 2007, **101**, 114903.
35. C. Groves, J. C. Blakesley and N. C. Greenham, *Nano Lett.*, 2010, **10**, 1063.
36. C. Deibel, T. Strobel and V. Dyakonov, *Phys. Rev. Lett.*, 2009, **103**, 036402.
37. J. Zaumseil, C. Groves, J. M. Winfield, N. C. Greenham and H. Sirringhaus, *Adv. Funct. Mater.*, 2008, **18**, 3630.
38. C. Groves, O. G. Reid and D. S. Ginger, *Acc. Chem. Res.*, 2010, **43**, 612.
39. H. Yan, B. A. Collins, E. Gann, C. Wang, H. Ade and C. R. McNeill, *ACS Nano*, 2012, **6**, 677.
40. S. Swaraj, C. Wang, H. Yan, B. Watts, J. Luning, C. R. McNeill and H. Ade, *Nano Lett.*, 2010, **10**, 2863.
41. C. R. McNeill, S. Westenhoff, C. Groves, R. H. Friend and N. C. Greenham, *J. Phys. Chem. C*, 2007, **111**, 19153.
42. C. Groves, R. A. Marsh and N. C. Greenham, *J. Chem. Phys.*, 2008, **129**, 114903.
43. T. A. Bull, L. S. C. Pingree, S. A. Jenekhe, D. S. Ginger and C. K. Luscombe, *ACS Nano*, 2009, **3**, 627.
44. C. Groves, R. G. E. Kimber and A. B. Walker, *J. Chem. Phys.*, 2010, **133**, 144110.
45. R. G. E. Kimber, A. B. Walker, G. E. Schroder-Turk and D. J. Cleaver, *Phys. Chem. Chem. Phys.*, 2010, **12**, 844.
46. G. F. A. Dibb, T. Kirchartz, D. Credgington, J. R. Durrant and J. Nelson, *J. Phys. Chem. Lett.*, 2011, **2**, 2407.
47. B. A. Gregg, *J. Chem. Phys. Lett.*, 2011, 3013.
48. C. Groves and N. C. Greenham, *Phys. Rev. B*, 2008, **78**, 155205.
49. B. A. Collins, J. R. Tumbleston and H. Ade, *J. Chem. Phys. Lett.*, 2011, **2**, 3135.
50. W. Yin and M. Dadmun, *ACS Nano*, 2011, **5**, 4756.

51. X. M. He, F. Gao, G. L. Tu, D. Hasko, S. Huttner, U. Steiner, N. C. Greenham, R. H. Friend and W. T. S. Huck, *Nano Lett.*, 2010, **10**, 1302.
52. R. Q. Png, P. J. Chia, J. C. Tang, B. Liu, S. Sivaramakrishnan, M. Zhou, S. H. Khong, H. S. O. Chan, J. H. Burroughes, L. L. Chua, R. H. Friend and P. K. H. Ho, *Nat. Mater.*, 2010, **9**, 152.
53. P. E. Keivanidis, V. Kamm, C. Dyer-Smith, W. Zhang, F. Laquai, I. McCulloch, D. D. C. Bradley and J. Nelson, *Adv. Mater.*, 2010, **22**, 5183.
54. R. A. Marsh, J. M. Hodgkiss, S. Albert-Seifried and R. H. Friend, *Nano Lett.*, 2010, **10**, 923.
55. D. P. McMahon, D. L. Cheung and A. Troisi, *J. Chem. Phys. Lett.*, 2011, **2**, 2737.
56. E. Helfand and Y. Tagami, *J. Chem. Phys.*, 1972, **57**, 1812.
57. X. Liu, S. Huettner, Z. Rong, M. Sommer and R. H. Friend, *Adv. Mater.*, 2012, **24**, 669.
58. A. R. Campbell, J. M. Hodgkiss, S. Westenhoff, I. A. Howard, R. A. Marsh, C. R. McNeill, R. H. Friend and N. C. Greenham, *Nano Lett.*, 2008, **8**, 3942.